

Statistical analysis of normal and abnormal dissymmetry in volumetric medical images

J.-P. Thirion^{a,*}, S. Prima^a, G. Subsol^a, N. Roberts^b

^aINRIA, Équipe EPIDAURE, Sophia-Antipolis, France

^bMARIARC, University of Liverpool, Liverpool, UK

Received 5 December 1997; received in revised form 10 October 1998; accepted 9 April 1999

Abstract

We present a general method to study the dissymmetry of anatomical structures such as those found in the human brain. Our method relies on the estimate of 3D dissymmetry fields, the use of 3D vector field operators, and T^2 statistics to compute significance maps. We also present a fully automated implementation of this method which relies mainly on the intensive use of a 3D non-rigid inter-patient matching tool. Such a tool is applied successively between the images and their symmetric versions with respect to an arbitrary plane, both to realign the images with respect to the mid-plane of the subject and to compute a dense 3D dissymmetry map. Inter-patient matching is also used to fuse the data of a population of subjects. We then describe three main application fields: the study of the normal dissymmetry within a given population, the comparison of the dissymmetry between two populations, and the detection of the significant abnormal dissymmetries of a patient with respect to a reference population. Finally, we present preliminary results illustrating these three applications for the case of the human brain. © 2000 Elsevier Science B.V. All rights reserved.

Keywords: Asymmetry; Dissymmetry; Brain; Medical image processing; Handedness

1. Introduction

The *Bauplan* or organizational scheme of many animal species is based on bilateral symmetry. This is the general case for the chordates and therefore vertebrates (fish, reptiles, mammals, etc.), insects, crustaceans, and many other groups. Some organs appear in pairs in the body, ‘symmetrical’ with respect to the mid-plane. This is the case for the limbs, eyes, ears and antennas in these species. Other organs are placed near the mid-plane and are also approximately symmetrical (nose, tail, etc.). This symmetry is rather general for the human head, including the brain and its two hemispheres. However, some organs such as the liver, which have no corresponding symmetrical structure, are *asymmetrical*.

Symmetrical anatomical structures, or paired structures, are sometimes also *dissymmetrical*¹ which means that they are roughly symmetrical but each of the two organs in a pair can represent a specialization and therefore a slightly different morphology. Shellfish, such as lobsters, present a striking example of lateral specialization. Of their pair of claws, the left claw is very robust and is used to crush mollusks (the ‘hammer’), and the right claw is slender and is used for shredding (the ‘scissors’). This dissymmetry is genetic and in a given lobster species, normal individuals always have the same laterality (i.e., the ‘hammer’ claw on the left and the ‘scissors’ claw on the right). With respect to a given population, a ‘normal’ dissymmetry is a dissymmetry that is ‘significantly distinct’ from a perfect symmetry

*Corresponding author. Current address: FOCUS Imaging S.A., ‘Les Genêts’, 449 Route des Crêtes, Sophia-Antipolis, 06560 Valbonne, France. Tel.: +33-492-38-8814; fax: +33-492-38-9646.

E-mail address: jpthirion@focus-fr.com (J.-P. Thirion)

¹Dissymmetry (Merriam–Webster) means a deficiency in symmetry, whereas asymmetry means a lack of symmetry (‘a-’ = without). We make this important semantic distinction in this paper.

for this population: a precise statistical definition of this will be given.

The normal dissymmetry can be studied *per se*. For the human brain, some normal functional asymmetries are well known (as early as the work of Paul Broca (1865)), which translate into morphological asymmetries/dissymmetries of the brain. From Crow (1993), also referring to Geschwind and Levitsky (1968): “. . . there are structures in the left temporal lobe, including the planum temporale, which forms part of the superior temporal gyrus, that are larger on the left than on the right. These encompass those areas of association cortex, including Wernicke’s area, that are responsible for speech and communication”. The dissymmetry in this case is tentatively attributed to the cerebral dominance gene (see Annett, 1985; McManus, 1985).

However, due to the lack of precise morphometric tools, the question as to what extent functional asymmetries translate into measurable morphological dissymmetries remains controversial. One aim of the present paper is to propose a new morphometric tool for addressing this issue.

The quantification of abnormal dissymmetry can also be a powerful tool to detect abnormalities. This is an alternative to the comparison of an individual to the average and standard deviation values measured in a population of normal specimens. Sometimes, the inter-individual variations in the normal population are so high (for example, brain ventricle volume variations) that they prevent a clear detection of abnormalities. In that case, comparing the relative dissymmetry measures of a patient to a population can give more relevant information than comparing absolute sizes (for example, comparing the ratio of the volumes of the two lateral ventricles instead of comparing directly the absolute ventricle volumes). However, the normal and abnormal components of the dissymmetry must still be identified in order to detect and quantify the abnormality itself. Hence population studies are also strongly needed in the analysis of the dissymmetry in a single patient to find statistically significant relative differences rather than absolute differences. This is the second purpose of this paper. A typical question can be: is the dissymmetry of the lateral ventricles in a patient significantly higher than the normal dissymmetry of a control population?

We present a new method to evaluate the normal and abnormal dissymmetry of symmetrical organs such as the human brain. Our method allows for the automatic detection of the mid-plane in the 3D images and the alignment of the image with respect to a fixed direction. We show how to compute and fuse the dissymmetry information of a population and also how to determine the regions which are significantly dissymmetrical (i.e., with respect to perfect symmetry). Then, we show that the dissymmetry field of several populations can be measured and compared, and that the regions with significantly different dissymmetry can be outlined. Lastly, we present preliminary experimental results for a variety of questions,

such as the normal dissymmetry of human brains, and the comparison of brains of left- and right-handed people, the comparison of an epileptic and a patient with a focal aphasia to a normal population.

2. Existing work about dissymmetry

Asymmetry and dissymmetry have already been extensively studied in the medical field (see for example (Davidson and Hugdahl, 1994), for a review of some of these studies). There is, for example, a great deal of work dealing with abnormal dissymmetry of the human brain in the case of schizophrenia (see DeLisi et al., 1997). Here, we will not discuss the medical relevance of these studies but will focus instead on the geometrical aspects of their methods.

A common feature is that these studies, performed by specialists in anatomy or neurology, generally follow very strict clinical protocols. These protocols are set to avoid statistical ‘pollution’ due to parameters such as sex, age, height, handedness, unrelated to the question which is asked but which can have an influence on dissymmetry. The careful setting of these experiments requires a lot of theoretical and practical work in addition to profound medical expertise. Another common feature is that the statistics are deeply involved, using tests such as Student’s or Hotelling’s tests or *t*-tests.

However, the geometric aspect of the problem is generally not handled properly. The definition of homologous features in both sides of the anatomical structure is generally performed manually, which is a time consuming and tedious task, and creates a sensitivity with respect to the operator. This variability has to be evaluated by intra- and inter-observer variability analyses. Also, the geometric representations which are used, are generally very crude and the huge amount of information available in 3D medical images is reduced to very poor data. For example, the ‘lengths’ or ‘widths’, of anatomical structures viewed in projection, such as the length of the ventricles in the case of air encephalographic studies (see Jacobi and Winkler, 1927; Hunter et al., 1968). In other cases, structures are studied independently slice by slice in MR images or cryogenic sections, with the underlying assumption that the slices are exactly perpendicular to the mid-plane, and that there is no difference in symmetry along the axial direction. By not taking the 3D information fully into account, many studies are not conclusive simply because the dissymmetry information is lost due to measurement errors.

Although we are using basic principles of statistical analysis similar to traditional ones, our method is new in that we attempt to use the geometric information present in the entire 3D image. We apply 3D elastic matching to match both sides of the object and 3D vector field analysis techniques to perform the statistical analysis. This is

different from methods where segmentation tools are used independently to process both sides of the object before the two sets of shapes are finally compared. In our method, segmentation is optionally used and only at the end of the process in order to present or synthesize the dissymmetry information into a few parameters (a few volume variation measures of organs, see (Thirion and Calmon, 1997)).

There are some similarities between our work and (Marias et al., 1996). In the latter, the mid-plane is automatically detected from the brain images using 2D snakes which are propagate through the slices to obtain a set of 2D mid-lines. A 3D plane is fitted to the set of mid-lines by a least-squares technique and the 3D image is realigned with respect to it. The cortical surface is also extracted using a propagation of 2D snakes, and the perpendicular distance from the mid-plane to the cortical surface is measured for both sides, leading to a pictorial representation of the mid-plane, colored with dissymmetry values. Finally, the information of several subjects are fused, using a surface to surface-matching technique based on the cortical surface.

Our method is similar to Marias et al. (1996) in that the mid-plane is computed, the images are realigned and non-rigid matching is used to perform inter-patients data fusion. However, several other aspects are very different: we are using a volumetric matching technique instead of surface segmentation and surface matching. In particular, we determine the symmetry plane by a least-squares fitting from features matched in both object sides instead of trying to detect the inter-hemispheric fissure of a brain. Our symmetry plane therefore has a different definition that is much less sensitive to the flatness of the inter-hemispheric fissure and is in fact, not at all specific to brain images. Another difference is that our dissymmetry map is defined everywhere in the 3D volume (a 3D image), whereas it is only defined in the mid-plane in (Marias et al., 1996) (a 2D image). Accordingly, inter-patients data fusion is fully volumetric, allowing for local analysis of the differences. Lastly, we will see that we are able to indicate effects such as relative local expansions or atrophies, whereas only brain width differences can be measured in (Marias et al., 1996).

3. The computation of dissymmetry maps

3.1. Symmetry, chirality and mid-plane

*Chirality*² is associated with symmetry: more precisely, two chiral objects are symmetrical with respect to a plane but up to a rigid transform.

For example, two hands are chiral which means that after a proper rigid placement (i.e., by joining them), they

are approximately symmetrical with respect to a plane. Such anatomical structures have no symmetry plane per se, but we will see that their dissymmetry can be studied anyway, thanks to the 3D deformation field obtained between the image of one structure and a symmetric version of the corresponding chiral structure.

For some other structures, such as the brain, we can reasonably assume the existence of a symmetry plane that we call the *mid-plane*. As we will see, this constraint can be taken into account explicitly in the matching process that determines the correspondence between the two sides of a symmetrical object. Furthermore, the image of a symmetrical object can be realigned, that is, the mid-plane of this object can be placed according to a given arbitrary plane.

3.2. Automatic realignment of a symmetrical object

Our realignment method is based on the extensive use of non-rigid matching tools developed to perform 3D inter-patient matching. Examples of such tools can be found in (Christensen et al., 1994; Gee et al., 1993; Thirion, 1998). For a given image I_1 , we assume that the object is roughly symmetrical and that a direction approximately perpendicular to the mid-plane is known, which is a reasonable assumption for medical images such as 3D brain images. If (x, y, z) are the principal axes of the 3D space, we assume for example that this is the x axis.

The first step is to choose an arbitrary plane P' in the original image to compute a chiral image $K(I_1)$ (see Fig. 1). If t_x is the number of voxels in the x direction, this plane can be

$$P':x = t_x/2. \tag{1}$$

A non-rigid technique, applied between I_1 and $K(I_1)$, gives couples $\{(p_i, p'_i)\}$ of corresponding points ($\{p_i\} \subset I_1$ and $\{p'_i\} \subset K(I_1)$). The couples $\{(p_i, p''_i)\}$ where $p''_i = K^{-1}(p'_i) = K(p'_i)$ represent therefore corresponding points

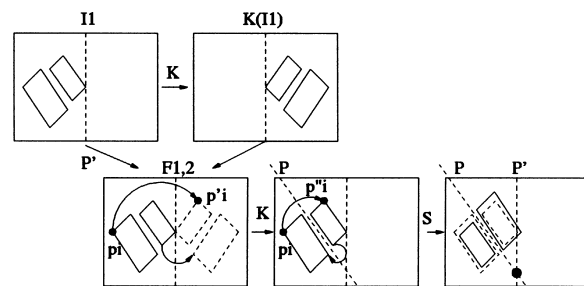


Fig. 1. Basic principle of the mid-plane determination: the image I_1 is transformed into a symmetrical image $K(I_1)$ with respect to an arbitrary plane P' (therefore $K = K^{-1}$). Then a point to point correspondence $F_{1,2}$ is computed between both images, leading to pairs (p_i, p'_i) . Applying K to the p'_i points gives couples (p_i, p''_i) of corresponding points with respect to the mid-plane P , which are used to compute the final symmetry S or equivalently the mid-plane P itself.

²From the Greek *Kheir*; the hand.

between both sides of the object (for example between the brain hemispheres).

The second step is to compute a symmetry S_p , characterized by its plane P , which means three parameters in 3D (the normalized normal to the symmetry plane: two parameters and the distance to the origin: one parameter), that minimizes a criterion C :

$$C = \sum_i (S_p(p_i'') - p_i)^2 = \sum_i (S_p \circ K(p_i') - p_i)^2. \quad (2)$$

It can be demonstrated that P is going through the barycenter $G = 1/2n(\sum_i p_i + \sum_i p_i'')$ of the two sets of n points $\{p_i; p_i''\}$ and that its normal n is the eigenvector associated with the smallest eigenvalue of the following matrix I :

$$I = \sum_i (p_i - G)(p_i'' - G)^T. \quad (3)$$

In particular, this plane P is not the plane which interpolates $\{p_i; p_i''\}$ with least-squares minimization based on distances. If we note $R = S \circ K$, then R is an affine rotation whose rotation axis is the intersection of planes P and P' .

Determining S (three parameters) is therefore equivalent to evaluating the affine rotation³ R , having a rotation axis in P' , that minimizes the least-squares distance between $\{p_i\}$ and $\{p_i'\}$ or, in other words, that maximizes the similarity between I_1 and $K(I_1)$. This gives other practical ways to evaluate S : for example, R can be evaluated directly by using mutual information minimization techniques (see Viola and Wells, 1995; Maes et al., 1997) adapted to affine rotations with axes in P' and applied between I_1 and $K(I_1)$. The symmetry plane P is the mid-plane of the object in I_1 .

We can then demonstrate that $R^{1/2}$, the affine rotation having the same axis as R but effecting half the rotation angle, is a rigid transform whose inverse ($R^{-1/2}$) can be used to realign the mid-plane with the arbitrary plane P' . An example of this realignment of a real image is shown in Fig. 2 (see Fig. 3).

- if R is evaluated directly (image-based minimization techniques), $R^{1/2}$ is conveniently determined by decomposing R into a translation t and a vectorial rotation represented by its rotation vector r (whose norm is the rotation angle and whose direction is the rotation axis). The rotation in $R^{1/2}$ is then $r/2$ and the translation is $(r/2 + Id)^{-1}(t)$ (Id is the identity transform).
- if the symmetry plane P is evaluated directly (corresponding points techniques), it is more convenient to determine $R^{1/2}$ from the intersection of the symmetry planes P of S and P' of K and the angle between them.

³An affine rotation is defined by five parameters: the rotation axis, which is a 3D line (four parameters) and a rotation angle. The constraint that this rotation axis has to be within a given plane P' reduces the number of free parameters to three only, exactly as it is the case for the symmetry S .

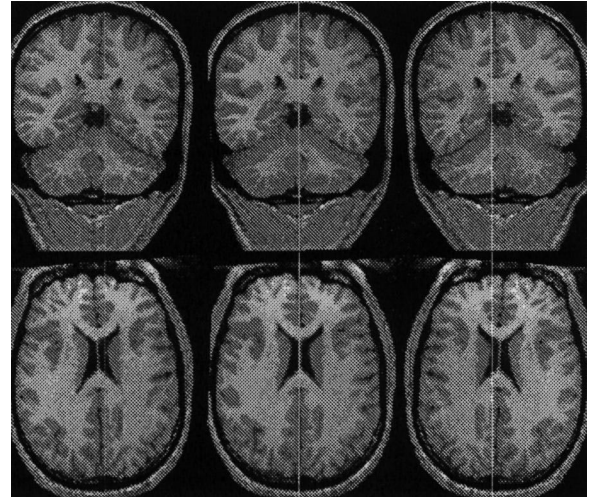


Fig. 2. This image presents the result of the application of our automatic 3D realignment tool. On the left: coronal and axial view of the same patient of the original image I_1 . On the right: the chiral image $K(I_1)$. In the middle: the realigned image $R^{-1/2}(I_1)$. The vertical white line is plane P' : $x = t_x/2$.

Then a re-sampling method such as tri-linear interpolation can be applied to transform image I_1 into the realigned image $I_1' = R^{-1/2}(I_1)$.

3.3. Dissymmetry field computation

A practical feature of most non-rigid inter-patient matching techniques is that the final result is sensitive to the original relative position of the two objects to be matched. To reduce this distance in the case of a symmetrical object, we propose to compute the dissymmetry field by applying the non-rigid matching technique between the realigned image I_1' and its chiral version $I_2' = K(I_1')$ instead of directly between I_1 and $K(I_1)$.

If the objects to be compared are chiral but not symmetrical (hands for example) and imaged separately (I_{left} for the left hand and I_{right} for the right hand), we propose to compute first the non-rigid correspondence between I_{left} and $K(I_{right})$. From these corresponding points, we deduce a rigid transform R by a conventional least-squares method (using for example a quaternion representation of the rotations or a rotation vector representation and Kalman filtering to reject outliers; see Ayache, 1991). Finally, we re-sample one of the two images with R : $I_1' = R^{-1}(I_{left})$ is made superimposable to

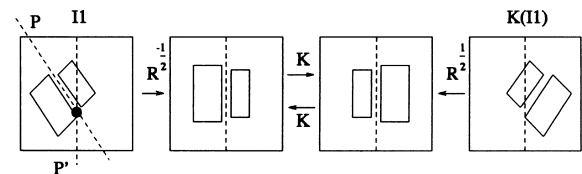


Fig. 3. The transform $R^{-1/2}$, where $R = S \circ K$ and $R^{1/2} \circ R^{1/2} = R$ can be used to realign the mid-plane P with the arbitrary plane P' .

$I'_2 = K(I_{\text{right}})$ or, for symmetry, we can re-sample both left and right images $I'_1 = R^{-1/2}(I_{\text{left}})$ and $I'_2 = R^{1/2}(K(I_{\text{right}}))$. If $R:(\mathbf{r},\mathbf{t})$ then we still have

$$R^{1/2}:(\mathbf{r}/2,(\mathbf{r}/2 + Id)^{-1}(\mathbf{t})). \quad (4)$$

and $R^{1/2} \circ R^{1/2} = R$. We note that we have exactly the same formulation as in the case of a symmetrical object, except that R is no longer constrained to be an affine rotation but is a general rigid displacement (six parameters). After the realignment step, a *dissymmetry field* is computed between I'_1 and I'_2 , and for either case (symmetrical or simply chiral).

3.4. Implementation

For our experiments and for both the realignment and the dissymmetry field computation, we have used a non-rigid matching method based on ‘demons’ (see Thirion, 1998), whose output is a dense 3D deformation field $F_{1,2}$ between the two images, that is, for each voxel $p_i:(x,y,z)$ in image I'_1 , we have three offsets (d_x, d_y, d_z) which give the corresponding point $p'_i:(x+d_x, y+d_y, z+d_z)$ in $K(I'_1)$. A nice feature of this algorithm is that it provides a ‘bijective’ deformation field in the sense that it also computes an inverse deformation field $F_{2,1}$, where $F_{2,1} \circ F_{1,2}$ is very close to identity (not exactly equal because we are processing discrete vector fields).

We note, however, that even for the case of an almost symmetrical object, the computed dissymmetry field $F_{1,2}$ is not exactly symmetrical with respect to P' . This is mainly because the origins of the vectors on both sides are different, as explained in Fig. 4: we have $F \neq K(F)$, but $F = K(F^{-1})$. We have explicitly used this last constraint in our non-rigid matching method when processing symmetri-

cal objects such as brains: more precisely, we set $F_{2,1} = K(F_{1,2})$ at each iteration of our matching method and then we redistribute the residual error $F_{2,1} \circ F_{1,2}$ to both deformation fields, which leads to better results and better coherency between $F_{1,2}$ and $F_{2,1}$.

4. The analysis of dissymmetry fields

We now discuss multiple ways to perform the analysis of dissymmetry fields. We first concentrate on the type of information which can be obtained from a single patient’s image and then on how statistical analyses can be performed with respect to one or several populations.

4.1. The case of a single specimen

Several different vector field operators can be applied to a dissymmetry field in order to obtain a 3D scalar image, which can then be visualized. A simple one is the norm of the vector field $\|F\|$, which emphasizes without distinction many types of dissymmetry, displaced structures as well as shearings, expansions or atrophies.

To be more specific, dedicated operators can be used: for expansions or atrophies, we found in the case of temporal evolution studies of lesions that an interesting operator is $\|F\|\text{div}(F)$, that is, the norm times the divergence of the vector field (see Thirion and Calmon, 1997). We found experimentally (in (Thirion and Calmon, 1997) also) that this operator more robust to compute than the norm of the Jacobian, but other operators could be applied. For $\|F\|\text{div}(F)$, the idea is that the norm characterizes the magnitude of the deformation, which holds also for large translations, while the divergence characterizes its radial aspect which can also be important in noisy regions. The combination of high divergence and high magnitude is a feature very characteristic of atrophies or expansions due, for example, to lesions or cancer growths. Our operator gives a very high response to such phenomena. We have also developed very precise stereological methods to evaluate quantitatively the volume variation, again for time series (also in Thirion and Calmon, 1997), that can be applied almost directly to the case of dissymmetry field analysis to evaluate quantitatively the relative sizes of symmetrical structures. Fig. 5 presents the result of the dissymmetry field and $\|F\|\text{div}(F)$ operator applied to a real patient.

We have selected the region of the temporal lobes for the display (but the dissymmetry field is really 3D) because this region is very dissymmetrical in this subject (a young right-handed healthy man) and, as we will see, in the majority of the subjects. In the $\|F\|\text{div}(F)$ image, white represents an expansion, which means a larger structure while black represents a smaller structure and grey a symmetrical structure. Hence the subject’s right temporal lobe (on the left in the image) is larger than his left

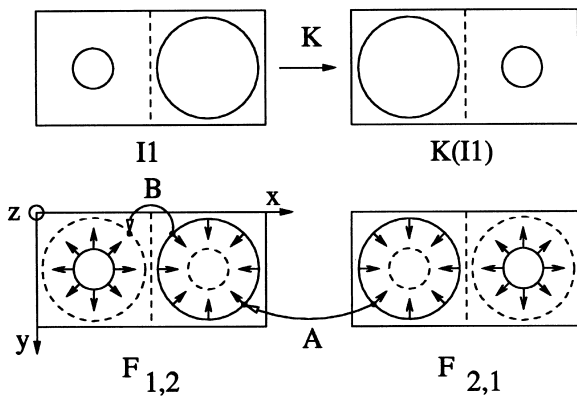


Fig. 4. This figure illustrates why $F \neq K(F)$ and $F = K(F^{-1})$. The image I_1 is transformed into $K(I_1)$. The direct deformation $F_{1,2}$ (the discrete approximation of F) is computed between I_1 and $K(I_1)$ and the reverse transformation $F_{2,1}$ (the discrete approximation of F^{-1}) between $K(I_1)$ and I_1 . At a given point p (see the arrow A), if $f_{1,2}:(d_x, d_y, d_z)$ then $f_{2,1}$ in $K(p)$ is $(-d_x, d_y, d_z)$. But $f_{1,2}$ in $K(p)$ has no reason to be exactly $(d_x, -d_y, -d_z)$, because the origins of the two vectors are not the same (see arrow B).

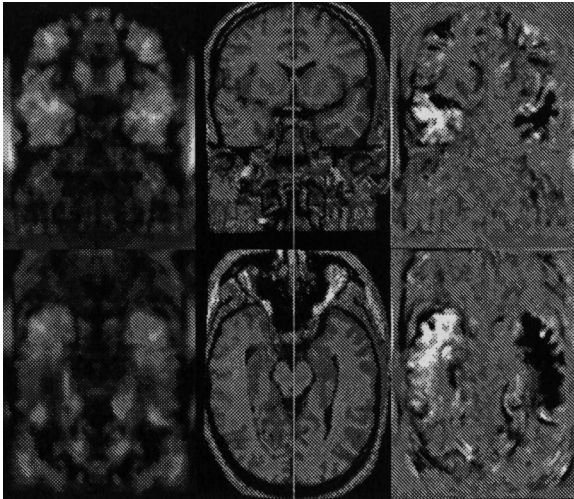


Fig. 5. This figure illustrates the dissymmetry field computation (left, norm of the field) and the application of the $\|F\|\text{div}(F)$ operator (right) on the realigned image of a real subject (middle). Note that the dissymmetry field is a 3D image (here, only a coronal and an axial section of the same 3D image are presented).

temporal lobe, which is a known normal dissymmetry in this population (see for example (Bilder et al., 1994)). This does not mean that some sub-structures of the temporal lobe are not larger on the left than on the right, as mentioned previously (see also (Crow, 1993)), but the total volume seems to be larger on the right side. Also, the dissymmetry seems to be located mainly in the white matter.

However, as stated in Section 1, one has to establish precisely the normal and abnormal components of the dissymmetry in order to provide a useful diagnosis. This means comparing a subject to a reference population. For example, we will see later that the dissymmetry of the temporal lobes that we observe for this particular subject is confirmed to be normal, based on a comparison with a database of 10 right-handed healthy men.

4.2. Inter-patient fusion

Again, non-rigid inter-patient matching is used to perform data fusion between different subjects, using the same scheme as presented in (Thirion et al., 1996). A reference specimen's image I_r is chosen and realigned, and the deformation fields $F_{i,r}$ from all the realigned images I_i of specimens i to the reference image I_r are computed. The dissymmetry fields of the realigned images are then computed and an operator may be applied to this field before the result is projected onto the reference specimen's image (see Fig. 6). Once more, we have used the non-rigid matching method described in (Thirion, 1998) to fuse the different specimens, and we have studied either the averaged dissymmetry vector field or the averaged result of the $\|F\|\text{div}(F)$ operator.

The first- and second-order statistical parameters are

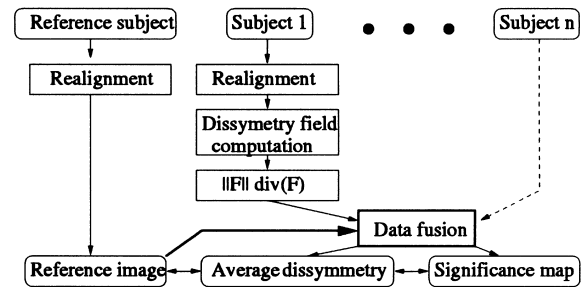


Fig. 6. Fusion of the data: the images of all patients are realigned, and the dissymmetry field and norm \times divergence operator are computed. Then, all the dissymmetry maps are projected onto the realigned image of a reference specimen. Lastly, the dissymmetry field and the significance map can be compared point by point to the reference image in order to determine which anatomical structure is significantly dissymmetrical.

computed for each voxel of the reference image, using the projected values of the whole population (mean and variance for $\|F\|\text{div}(F)$, or mean and covariance matrix for the vector field F , with one covariance matrix per voxel).

Finally, individual specimens or other population specimens can be projected onto the reference patient and compared with the reference population statistics to determine significant differences.

4.3. Statistical maps and statistical tests

Different types of questions can be addressed, leading to different statistical maps and tests. The principal questions are:

- what regions in a given population are significantly dissymmetrical?
- What regions in a given population have a significantly different dissymmetry than similar regions in another given population?
- What regions of a given specimen are significantly different from the normal dissymmetry of a population?

In each case, a probability map can be computed via the application of the inverse of the Fisher–Snedecor or F -function to a Mahalanobis distance or T^2 value (see for example (Anderson, 1958; Thompson and Toga, 1997)). We consider here the multivariate case where the samples are random vectors of dimension p and are supposed to have a Gaussian distribution. When dealing with 3D dissymmetry fields, we have $p = 3$ and if the $\|F\|\text{div}(F)$ operator is used then $p = 1$ (univariate case).

4.3.1. A significant dissymmetry

The first question is typical of pure anatomical studies. The aim can be, for example, to designate the regions of the brain in a population of right-handed young, healthy males which are significantly dissymmetrical (with respect to perfect symmetry, i.e., a null dissymmetry field). This is a classical multivariate analysis test. For a given voxel x in the reference image, the random vector for a specimen i projected in x being x_i , the average on the population of n

specimens being $\boldsymbol{\mu}$ and the covariance matrix being $\boldsymbol{\Sigma}$, we have

$$\boldsymbol{\mu} = \frac{1}{n} \sum_{i=1}^n x_i, \quad (5)$$

$$\boldsymbol{\Sigma} = \frac{1}{n-1} \sum_{i=1}^n (x_i - \boldsymbol{\mu})^T (x_i - \boldsymbol{\mu}).$$

The probability of being wrong in saying that the population has a mean different from $\boldsymbol{\mu}_0=0$ (i.e., is different from a perfect symmetry) is called the α value and is given by the following formula:

$$\alpha = F_{p,n-p}^{-1} \left[\frac{(n-p)}{(n-1)p} T^2(\boldsymbol{\mu}_0) \right], \quad (6)$$

where

$$T^2(\boldsymbol{\mu}_0) = n(\boldsymbol{\mu} - \boldsymbol{\mu}_0)^T \boldsymbol{\Sigma}^{-1} (\boldsymbol{\mu} - \boldsymbol{\mu}_0). \quad (7)$$

The closer the α value is to zero, the more significant the dissymmetry. The α values computed for all voxels can be represented in a 3D image. Setting a threshold α_0 in this image (for example $\alpha_0 = 0.001$) is equivalent to performing an Hotelling's test, that is, to determine the voxels where T^2 is such that

$$T^2 > T_0^2 = \frac{(n-1)p}{(n-p)} F_{p,n-p}(\alpha_0). \quad (8)$$

α_0 is called the significance level of the test. It is, however, unfortunate to reduce the information to only a binary image. To have a more pictorial representation of the map of α values, we propose to display the following values:

- if $(\alpha > \alpha_0)$ then $i = \alpha_0/\alpha$,
- else $i = 1$.

The output is a 3D image coded with floating point values where the intensity i is between 0 and 1, and saturated ($i = 1$) when the dissymmetry is highly significant. The Hotelling's test is then simply to determine the voxels $i = 1$ in such an image. In the case of expansion/contraction, the sign of the divergence can be used to provide additional information on the nature of the dissymmetry, to lead to an image with $i \in [0,1]$, where $i = 0$ (black) means significantly smaller (with a significance level α_0), $i = 0.5$ (gray) means undetectable dissymmetry and $i = 1.0$ (white) means significantly larger (also with a significance level α_0).

4.3.2. Significant dissymmetry differences between populations

Our second question is typical of pathological studies where, other parameters being controlled, a population of n_1 pathological or atypical subjects $\{x_{1,i}\}$ with mean $\boldsymbol{\mu}_1$ is compared to a population of n_2 controls $\{x_{2,i}\}$ with mean $\boldsymbol{\mu}_2$. It can be for example a population of right-handed schizophrenic males with a population of right-handed healthy males. The probability of being wrong in saying that the two populations have a different mean is

$$\alpha = F_{p,n_1+n_2-p-1}^{-1} \left[\frac{n_1+n_2-p-1}{(n_1+n_2-2)p} T^2(\boldsymbol{\mu}_1, \boldsymbol{\mu}_2) \right], \quad (9)$$

where

$$T^2(\boldsymbol{\mu}_1, \boldsymbol{\mu}_2) = \frac{n_1 n_2}{(n_1 + n_2)} (\boldsymbol{\mu}_2 - \boldsymbol{\mu}_1)^T \boldsymbol{\Sigma}^{-1} (\boldsymbol{\mu}_2 - \boldsymbol{\mu}_1),$$

$$\begin{aligned} \boldsymbol{\Sigma} = & \frac{1}{n_1 + n_2 - 2} \sum_{i=1}^{n_1} (x_{1,i} - \boldsymbol{\mu}_1)^T (x_{1,i} - \boldsymbol{\mu}_1) \\ & + \sum_{i=1}^{n_2} (x_{2,i} - \boldsymbol{\mu}_2)^T (x_{2,i} - \boldsymbol{\mu}_2). \end{aligned} \quad (10)$$

We note, however, that this formula is valid only under the hypothesis that the variances of the two populations of subjects (which are a priori unknown) are exactly the same, which is not always true, especially with respect to groups of diseased patients. What statistics can tell us is that for a 'reasonable' number of samples in both populations, this assumption is no longer needed. However, for reduced sets of samples and without the variance equality hypothesis, more complicated formulae have to be used (again, see (Anderson, 1958)).

4.3.3. Significant atypical dissymmetry

Our third question can be used for individual diagnosis. A typical question might be to detect automatically a brain tumor as being a region significantly more dissymmetrical than the same region in a normal population. The probability of being wrong in saying that a value x_0 is significantly different from a population having a mean $\boldsymbol{\mu}$ and a covariance matrix $\boldsymbol{\Sigma}$ is a simplification of the preceding formula for $n_2 = 1$:

$$F_{p,n-p}^{-1} \left[\frac{n-p}{(n-1)p} T^2(\boldsymbol{\mu}) \right], \quad (11)$$

where

$$T^2(\boldsymbol{\mu}) = \frac{n}{n+1} (\boldsymbol{\mu} - x_0)^T \boldsymbol{\Sigma}^{-1} (\boldsymbol{\mu} - x_0). \quad (12)$$

4.3.4. One-side and two-sides t-tests

Scalar fields such as $v = \|F\| \text{div}(F)$ correspond to a distribution with two tails (v is a signed value). The direct restriction of the multivariate analysis to the univariate case corresponds to determining if $|v - v_0|$ is statistically different from 0: the two sides of the distribution are tested simultaneously, which is called a two-sided t -test. Alternatively, we could have computed one-sided t -tests corresponding to places where v is significantly larger than v_0 (or where v is significantly smaller than v_0). In the rest of the paper, all the results which are presented are the results of two-sided t -tests, even if significant regions are colored in opposite colors depending on the sign of $v - v_0$, which was done only for pictorial representation. Two-sided t -tests underestimate one-sided t -tests by a factor of 2.

4.3.5. Partial conclusions about dissymmetry maps

Many combinations are possible, such as: is my patient closer to a group of epileptics than to a group of controls? The computations which have been presented here are valid for voxel to voxel uncorrelated measurements, which unfortunately is not the case in practice because the deformation field between the direct and chiral images is regularized. However, the spatial coherency can be used to derive more robust statistical parameters, as proposed by the theory of random fields and implemented in the SPM method in the case of the analysis of functional images (for example, see (Friston et al., 1990)). We have not yet investigated the possibilities of such a method in the case of dissymmetry studies; this appears to be an interesting perspective to explore.

5. Synthetic experiments

We have performed various tests to validate the different modules used in this method (see (Thirion et al., 1996) for a first validation of non-rigid inter-patient matching, or (Thirion and Calmon, 1997) for tests about volume variation quantification).

To validate the dissymmetry field computation, we have performed the following experiment: starting from the 3D image I_1 of a real patient, we have simulated an artificial expansion (a mass effect) at a known location and of a known radius in the right hemisphere of the brain (image D_1). We have artificially stretched the 3D image without altering the intensity. More precisely our deformation simulates a Jacobian of 2 (instead of 1) in a bounded spherical region, but, as we simulated incompressible material everywhere else, the effect of the stretching is

extending far from this original spherical region, leading to a detection which is less localized than with a bounded deformation. We have then computed the dissymmetry field F , $\|F\|$ and $\|F\|\text{div}(F)$ of D_1 (see Fig. 7), and compared it with the dissymmetry field obtained directly with I_1 .

The deformation can be seen visually by comparing I_1 and D_1 , but with D_1 alone, it is hard to determine visually the nature and amplitude of the deformation. In the $\|F\|$ images, there is a large region where the norm of the dissymmetry vectors are very high. It is therefore easy to detect that there is something unusual going on with respect to perfect symmetry, but it is, however, very difficult to determine the ‘cause’ of the dissymmetry, that is the focus of expansion. This focus can be emphasized only by using a vector field operator appropriate to expansion/atrophy. In the image presenting $\|F\|\text{div}(F)$, the expansion translates into a roughly spherical-shaped white region in the right hemisphere (on the left in the image), centered on the focus of expansion. Of course, it also translates into a symmetrical spherical dark region in the left hemisphere. The signal is less obvious in the outer boundary of the brain because it is corrupted by the natural dissymmetry of these regions. The ‘aperture’ problem, which states that deformation are easier to detect in directions perpendicular to interfaces (such as grey/white matter) than in parallel directions explains also why perfect spherical shapes are not retrieved.

In Fig. 8, we present the subtraction between I_1 images and D_1 images to emphasize the effects created by the expansion only. Again, only the $\|F\|\text{div}(F)$ provides a clear signal with respect to the localization and extension of the expansion. We hope to be able to emphasize with this technique the effect of a growing tumor such as a

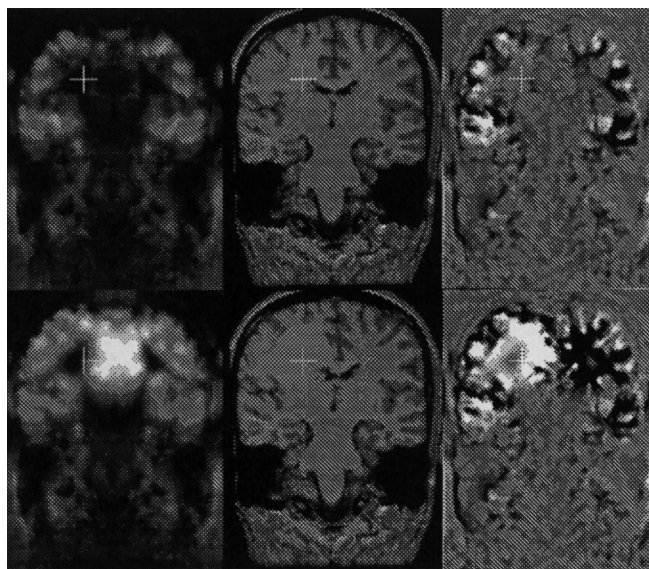


Fig. 7. Synthesized expansion in 3D within the brain of a healthy subject (top row, before expansion; lower, after expansion). Middle, original intensity images; left, $\|F\|$; and right, $\|F\|\text{div}(F)$. The crossbars represent the focal point of the expansion.

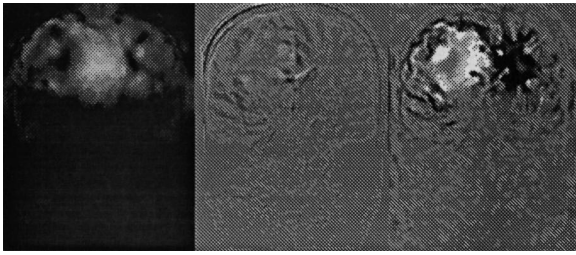


Fig. 8. Subtraction of images I_1 and images D_1 to emphasize the deformation effects only.

glioblastoma, which is very difficult to segment because of its diffusion within the tissue.

6. Some preliminary experimental results

The following results are very preliminary. In particular, they are not validated medical studies but are presented here only to illustrate the potential applications of our method. Much more work and strong collaborations with anatomists, along with much larger image databases are needed to lead to medically significant results.

6.1. A population of healthy right-handed males

A first experiment is on a population of 3D MR scans of 10 different healthy subjects, all of them being right-handed males. These subjects have been selected for the medical study described in (Mackay et al., 1998). Their handedness was ascertained using the Edinburgh Handedness Inventory (short form) which is a 10-item questionnaire giving a laterality quotient percentage from -100 (left handed) to 100 (right handed). Other metrics of handedness are described in (Holder, 1992). The 10 subjects rated a minimum of 87 with respect to this scale. We have realigned automatically all the images with respect to the mid-plane, computed their dissymmetry maps, applied the norm \times divergence operator and fused all the information in the frame of an eleventh subject's image (right-handed rating 100) also realigned, exactly as it was described in Section 4.3.1 and summarized in Fig. 6.

The results are presented in Fig. 9 for coronal and axial cross-sections and at the level of the temporal lobe only. The left images present the reference subject. The images in the middle present the average of $\|F\|\text{div}(F)$ for the 10 subjects. The significance map (the right images) present the loci which are significantly dissymmetrical (respectively, larger, white; or smaller, black). We have normalized the image of the significance map with a significance level $\alpha_0 = 0.001$ (that is, pure white or pure black means $\alpha \leq 0.001$). A mask has been applied to keep only the data at the level of the reference subject's brain. This experiment confirms that the dissymmetry map presented in Fig. 5 for a single subject is representative of a normal dissymmetry,

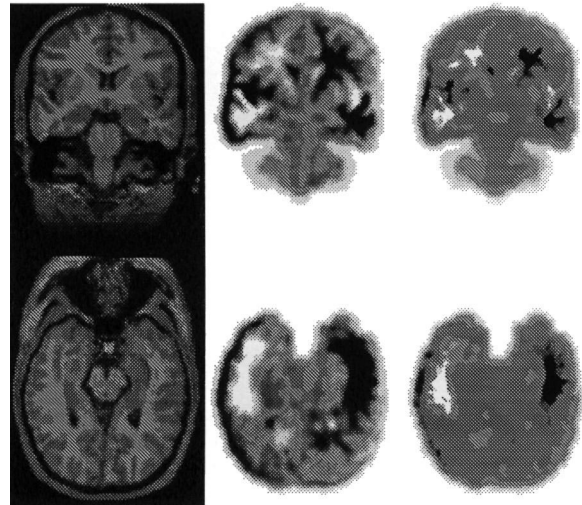


Fig. 9. Significant dissymmetry for a population of 10 healthy right-handed males. Left, reference patient; middle, average of the 10 $\|F\|\text{div}(F)$ maps; right, significance map for $\alpha_0 = 0.001$. The right temporal lobe (on the left in the image) is significantly larger than the left one for normal anatomy.

which means a larger right temporal lobe (on the left in the images) in normal subjects.

6.2. Left-handed versus right-handed subjects

We now illustrate what was presented in Section 4.3.2: the comparison of two populations. We have compared the average of 10 right-handed healthy males (handedness score ≥ 87) with the average of three left-handed healthy males (handedness score ≤ -57). The results are presented in Fig. 10, with the averages of $\|F\|\text{div}(F)$ for the right- and left-handed groups (left and middle images), and the significance map normalized using the same significance level α_0 as in Fig. 9 (the right images).

The results appear less conclusive than for normal dissymmetry. In particular, determining discriminant features of left-handed versus right-handed subjects is far from being evident. A careful exploration of the 3D data and more experiments with a larger set of right- and left-handed subjects are probably needed to lead to definitive conclusions.

6.3. A patient with focal aphasia

We now study a patient presenting a focal aphasia. In the image of this patient (Fig. 11), we note an obvious dissymmetry of the ventricles. The aim of this experiment is to retrieve this dissymmetry, based on the significance map and according to the methodology presented in Section 4.3.3. Fig. 11 presents coronal and axial views of the focal aphasic subject. On the left is the original image, in the middle is the $\|F\|\text{div}(F)$ dissymmetry map, and on the right is the significance map with respect to a popula-

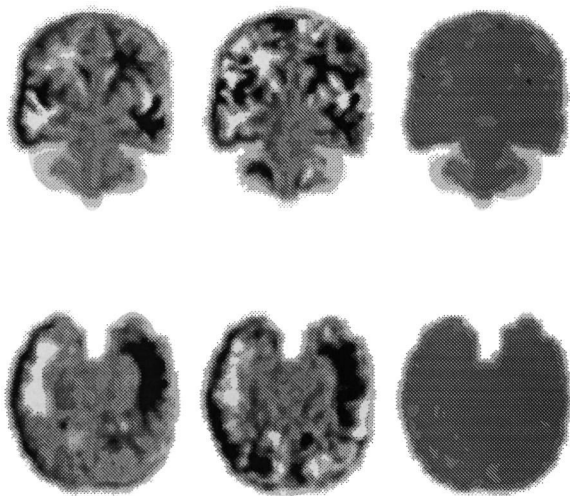


Fig. 10. Dissymmetries between a population of 10 right-handed males and a population of three left-handed males. Left, average of the 10 $\|F\|\text{div}(F)$ right-handed maps; middle, average of three left-handed maps; right, significance map for $\alpha_0 = 0.001$; the same significance level as for Fig. 9. These preliminary results are not conclusive with respect to a significant morphological difference between left- and right-handed people. Larger datasets are probably required before drawing any conclusion.

tion of 10 healthy right-handed males, projected back on the focal aphasic's image. The obvious dissymmetry of the brain ventricles is retrieved and correctly localized in the significance map, with very high magnitude significance values (using the same significance level as in Fig. 9).

6.4. A patient with focal epilepsy

We have performed exactly the same experiment for a

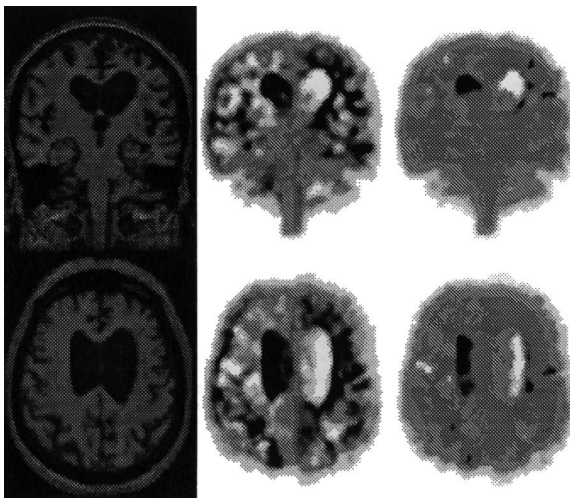


Fig. 11. Significant abnormal dissymmetry of a diseased patient (focal aphasia), with respect to the population of 10 right-handed normal males. Left, focal aphasic's image; middle, $\|F\|\text{div}(F)$ for the aphasic; right, significance map for $\alpha_0 = 0.001$, with respect to the 10 right-handed people. Note the significant dissymmetry at the level of the ventricles, which is correctly localized.

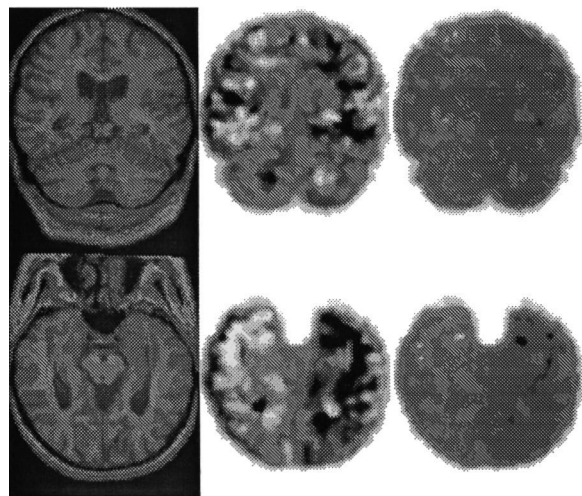


Fig. 12. Dissymmetry of a patient suffering from focal epilepsy, with respect to the population of 10 right-handed normal males. Left, focal epileptic's image; middle, $\|F\|\text{div}(F)$ for the epileptic; right, significance map for $\alpha_0 = 0.01$, with respect to the 10 right-handed people. A significant dissymmetry is hard to assess for this last case (note that the significance level is 0.01 in these images instead of 0.001). Again, more cases need to be studied.

focal epileptic patient (see Fig. 12), which could present an atrophy at the level of one of the hippocampi. The results, however, are less conclusive than for the case of the patient with focal aphasia (note that the significance map is normalized with $\alpha_0 = 0.01$ instead of 0.001 as in the other cases). We also expect that more experiments on a larger database of patients presenting the same disease (focal epilepsy) will enable us to be more precise in our conclusions.

7. Conclusion

We have presented a general method to study the dissymmetry of symmetrical organs, such as the human brain, using 3D dissymmetry fields, 3D vector field operators, and the computation of 3D significance maps. The main feature of our method is that we are dealing with dense volumetric representations of the dissymmetry. We have also proposed and tested a fully automated implementation of this method, relying mainly on 3D non-rigid inter-patient matching tools applied between the images and symmetric images with respect to an arbitrary plane. A by-product of this is an unsupervised method to realign automatically symmetrical structures with respect to their mid-plane. We have also described three main application fields, which are the study of the normal dissymmetry in a given population, the comparison of the dissymmetry between two populations, and the detection of the significant abnormal dissymmetries of a patient with respect to a reference population. Finally, we have presented preliminary results to illustrate these three applica-

tions for the case of the human brain. These must be investigated in depth, with the careful support of anatomists and for much larger databases to enable us to draw conclusive medical results.

Acknowledgements

Many thanks to Mrs Janet Bertot for a careful proofreading of the manuscript. This study also relates to the EC Biomed II project BIOMORPH, where we intend to use this method to study the dissymmetry of schizophrenic patients.

References

- Anderson, T.W., 1958. Introduction to Multivariate Statistical Analysis. Wiley, New York.
- Annett, M., 1985. Left, Right, Hand and Brain: The Right Shift Theory. Erlbaum, London.
- Ayache, N., 1991. Artificial Vision for Mobile Robots: Stereo Vision and Multisensory Perception. MIT Press, Cambridge, MA.
- Bilder, R.M., Wu, H., Bogerts, B., Degreef, G., Ashtari, M., Alvir, J.M.J., Snyder, P.J., Lieberman, J.A., 1994. Absence of regional hemispheric volume asymmetries in first-episode schizophrenia. *Am. J. Psychiatry* 151 (10), 1437–1447.
- Broca, P., 1865. Du siège de la faculté du langage articulé. *Bull. Soc. Anthropol.* 6, 377–393.
- Christensen, G.E., Rabbitt, R.D., Miller, M.I., 1994. 3D brain mapping using a deformable neuroanatomy. *Phys. Med. Biol.* 39, 609–618.
- Crow, T.J., 1993. Schizophrenia as an anomaly of cerebral asymmetry. In: Maurer, K. (Ed.), *Imaging of the Brain in Psychiatry and Related Fields*. Springer, Berlin, Heidelberg, pp. 1–17.
- Davidson, R.J., Hugdahl, K., 1994. *Brain Asymmetry*. A Bradford Book, Cambridge, MA.
- DeLisi, L.E., Sakuma, M., Kushner, M., Finer, D.L., Hoff, A.L., Crow, T.J., 1997. Anomalous cerebral asymmetry and language processing in schizophrenia. *Schizophr. Bull.* 232, 255–271.
- Friston, K.J., Frith, C.D., Liddle, P.F., Dolan, R.J., Lammertsma, A.A., Frackowiak, R.S.J., 1990. The relationship between global and local changes in pet scans. *J. Cerebral Blood Flow Metab.* 10, 458–466.
- Gee, J.C., Reivich, M., Bajcsy, R., 1993. Elastically deforming 3D atlas to match anatomical brain images. *J. Comput. Assist. Tomogr.* 17 (2), 225–236.
- Geschwind, N., Levitsky, W., 1968. Left-right asymmetry in temporal speech region. *Science* 161, 186–187.
- Holder, M.K., 1992. Hand Preference Questionnaires: One Gets What One Asks For. M. Phil. Thesis. Department of Anthropology, Rutgers University, New Brunswick, NJ, USA.
- Hunter, R., Jones, M., Cooper, F., 1968. Modified lumbar air encephalography in the investigation of long stay psychiatric patients. *J. Neurol. Sci.* 6, 593–596.
- Jacobi, W., Winkler, H., 1927. Encephalographische studien an cronisch schizophrener. *Arch. Psychiatr. Nervenkr.* 8, 299–332.
- Mackay, C.E., Roberts, N., Mayes, A., Downes, J.J., Foster, J.K., Mann, D., 1998. An exploratory study of the relationship between face recognition memory and the volume of medial temporal lobe structures in healthy young males. *Behav. Neurol.* 11, 3–20.
- Maes, F., Collignon, A., Vandermeulen, D., Marchal, G., Suetens, P., 1997. Multimodality image registration by maximization of mutual information. *IEEE Trans. Med. Imaging* 16 (2), 187–198.
- Marias, P., Guillemaud, R., Sakuma, M., Zisserman, A., Brady, M., 1996. Visualising cerebral asymmetry. In: Höhne, K.H., Kikinis, R. (Eds.), *Visualization in Biomedical Computing*. Vol. 1131 of Lecture Notes in Computer Science, Springer, Hamburg, Germany, pp. 411–416.
- McManus, I.C., 1985. Handedness, language dominance and aphasia: a genetic model. *Psychol. Med. Suppl.* 8, 140.
- Thirion, J.-P., 1998. Image matching as a diffusion process: an analogy with Maxwell's demons. *Medical Image Analysis* 2 (3), 243–260.
- Thirion, J.-P., Calmon, G., 1997. Measuring lesion growth from 3D medical images. In: *Nonrigid and Articulated Motion Workshop (NAM'97)*, Puerto Rico. IEEE.
- Thirion, J.-P., Subsol, G., Dean, D., 1996. Cross validation of three inter-patients matching methods. In: *Visualization in Biomedical Computing, VBC'96*. Vol. 1131 of Lecture Notes in Computer Science, Hamburg, Germany, pp. 327–336.
- Thompson, P.M., Toga, A.W., 1997. Detection, visualization and animation of abnormal anatomic structure with a deformable probabilistic brain atlas based on random vector field transformations. *Medical Image Analysis* 1 (4), 271–294.
- Viola, P., Wells, III W.M., 1995. Alignment by Maximization of Mutual Information. In: *Fifth Int. Conf. on Computer Vision, ICCV'95*, Cambridge, MA. IEEE, pp. 16–23.